

Improved Interpolated Dynamic DFT Synchrophasor Estimator Considering Second Harmonic Interferences

¹Lei Chen,¹Wei Zhao,¹Yiqing Yu,²Qing Wang, and ¹Songling Huang

¹Department of Electrical Engineering, Tsinghua University, Beijing, China
zhaowei@mail.tsinghua.edu.cn

²Department of Engineering, Durham University, Durham, UK

Abstract—The interpolated dynamic DFT (IpD²FT) is one of the most accurate dynamic synchrophasor estimation methods. But it suffers from infiltration from the second harmonic component. In this paper, the estimation errors of the IpD²FT caused by second harmonic interferences are firstly analyzed. Based on this, an improved interpolated dynamic DFT (IIPD²FT) synchrophasor estimator that considers second harmonic interferences are proposed. Multiple simulation tests show that, even under large second harmonic interference conditions, the IIPD²FT is much more accurate than the IpD²FT.

Index Terms—DFT, synchrophasor, second harmonic interference, spectral leakage, window function.

I. INTRODUCTION

Dynamic synchrophasor estimation is very useful and significant for power system monitoring and control. Traditionally, many researchers have paid attention to dynamic synchrophasor estimation under different dynamic conditions, such as power oscillations and frequency deviations, and a series of achievements have been made [1]–[4]. However, the second harmonic interferences, which may be significant in distribution networks [5], will also cause large estimation errors, especially when short length intervals are considered [6], [7]. As a result, it is necessary to study accurate synchrophasor estimation methods especially for second harmonic interference conditions.

The DFT can be used for synchrophasor estimation, and can sufficiently suppress harmonic interferences under synchronous sampling conditions. However, under non-synchronous sampling conditions, large errors will occur not only because of the spectral leakage but also because of the second harmonic interferences. Many improved DFT-based methods were proposed to reduce the error caused by spectral leakage [5], [6], [8]–[12], but these methods share a problem of no consideration of the second harmonic interferences. For example, the interpolated dynamic DFT (IpD²FT) synchrophasor estimator is a very useful and accurate tool to estimate dynamic synchrophasors [6]. However, when the second harmonic component is significant in a voltage/current signal, large errors will arise especially under large frequency deviation conditions.

A series of methods that consider second harmonic interferences were proposed to estimate dynamic synchrophasors,

such as the Taylor-Fourier transform (TFT), the improved Taylor weighted least square (ITWLS) method, and second harmonic filter Based method (SHFM) [7], [13], [14]. The TFT considers dynamic second harmonic components in the signal model, which can produce a notch-filter effect around the second harmonic frequency of the designed filter [13]. However, if under large frequency deviation conditions, the second harmonic interferences still cannot be clearly filtered. The ITWLS and SHFM can remove the second harmonic component in the signal model through two second harmonic measurement methods [7]. But these harmonic measurement methods suffer from the spectral leakage from the fundamental component.

Although the above methods can be used in various cases, this paper will focus on dynamic synchrophasor estimation under large second harmonic interference conditions. In this paper, an improved interpolated dynamic DFT (IIPD²FT) synchrophasor estimator for dynamic synchrophasor estimation is proposed. The estimation errors of the IpD²FT caused by the second harmonic component are firstly analyzed. Based on this, an improved synchrophasor estimation method that can sufficiently suppress second harmonic interferences in various cases is proposed.

II. ACCURACY ANALYSIS AND ENHANCEMENT OF THE IPD²FT

A. Brief Introduction of the IpD²FT

In general, a signal with the second harmonic component can be defined as

$$\begin{aligned} s(t) &= \sqrt{2}[a_1(t)\cos(2\pi ft + \varphi_1(t)) + a_2\cos(2\pi \cdot 2f \cdot t + \varphi_2)] \\ &= \sqrt{2}\text{Re}\{X(t)e^{j2\pi f_0 t}\} + \sqrt{2}a_2\cos(2\pi \cdot 2f \cdot t + \varphi_2) \end{aligned} \quad (1)$$

where $a_1(t)$ and $\varphi_1(t)$ are the magnitude (RMS value) and phase modulations of the fundamental component; a_2 and φ_2 are the magnitude and phase of the second harmonic, which are assumed as constant values; f and f_0 are the actual and nominal fundamental frequencies (50/60 Hz) respectively;

$$\begin{aligned} X(t) &= a_1(t)e^{j(\varphi_1(t)+2\pi\Delta ft)} \\ &= p(t)e^{j2\pi\Delta ft} \end{aligned} \quad (2)$$

is the synchrophasor, in which $\Delta f = f - f_0$ is the possible frequency deviation between f and f_0 , and $p(t)$ is the so called semi-synchrophasor.

Assuming the signal is sampled at a sampling rate $f_s = f_0 N_0$, and N_w samples are obtained in an observation window around time t_0 . Note that N_w should be an odd number to make t_0 lie in the center of the observation window. $c = \lfloor N_w/N_0 \rfloor$ is the nominal cycle number (integer) of the observation window. The Taylor series expansion is used to express $p(t)$ approximately, which is given by

$$p^K(t) = p_0 + \frac{n}{f_s} p_1 + \cdots + \frac{n^K}{K! f_s^K} p_K \quad (3)$$

$$-\frac{N_w - 1}{2} \leq n \leq \frac{N_w - 1}{2}$$

where p_k is the k th order derivative of $p(t)$ at time t_0 . Then, the approximate signal without consideration of the second harmonic component can be expressed as

$$s^K(t) = \frac{\sqrt{2}}{2} \sum_{k=0}^K \left[\frac{n^k}{k! f_s^k} p_k e^{j2\pi f t} + \frac{n^k}{k! f_s^k} p_k^* e^{-j2\pi f t} \right] \quad (4)$$

where $*$ denotes the conjugate operator. Applying the windowed DFT to (4) at a frequency f_b , it follows that

$$S^K(f_b) = \frac{\sqrt{2}}{N_w} \sum_{n=-(N_w-1)/2}^{(N_w-1)/2} s^K(n) w(n) e^{-j2\pi f_b n / f_s} \quad (5)$$

$$= \sum_{k=0}^K [p_k W_k(f_b - f) + p_k^* W_k(f_b + f)]$$

where

$$W_k(f_b) = \frac{1}{N_w} \sum_{n=-(N_w-1)/2}^{(N_w-1)/2} \frac{1}{k!} \left(\frac{n}{f_s}\right)^k w(n) e^{-j2\pi f_b n / f_s} \quad (6)$$

is a function corresponding to the adopted window $w(\cdot)$. By truncating the Taylor series to second order and applying the DFT to (4) at three different frequencies f_b , with $b = 1, 2, 3$, (5) can be rearranged as

$$\mathbf{S} \approx \mathbf{W}_R(f_b) \mathbf{P} + \mathbf{W}_I(f_b) \mathbf{P}^* \quad (7)$$

where \mathbf{S} is a column vector consisting of the DFT of the real signal at the three frequencies; \mathbf{P} and \mathbf{P}^* are two column vectors consisting of p_k and p_k^* , with $k = 0, 1, 2$; $\mathbf{W}_R(f_b)$ and $\mathbf{W}_I(f_b)$ are two matrixes consisting of $W_k(f_b - f)$ and $W_k(f_b + f)$, with $k = 0, 1, 2$ and $b = 1, 2, 3$. Then \hat{p}_0 and \hat{p}_1 can be obtained by solving (7), and the synchrophasor can also be estimated according to (2). Based on this, the fundamental frequency can also be estimated, which is given by

$$\hat{f} = f + \frac{f_s}{2\pi} \frac{\text{Im}\{\hat{p}_1 \hat{p}_0^*\}}{|\hat{p}_0|^2} \quad (8)$$

where $\text{Im}\{\cdot\}$ denotes the operation returning the imaginary part of the argument. Because the actual fundamental frequency is unknown, three iterations are needed to obtain high accuracy [6]. In the IpD²FT, the three frequencies used in

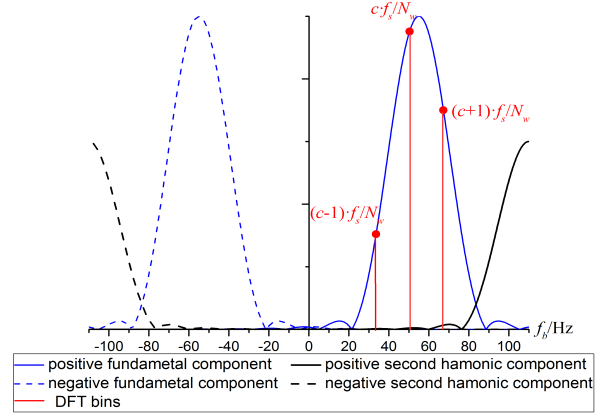


Fig. 1. The four components of the windowed DFT of $s(t)$. $c = 3$, $f_0 = 50$ Hz, $f = 55$ Hz, $N_0 = 40$, and the Hanning window are selected for the illustration.

the DFT are the bin frequencies, with $f_b = \frac{(c-1)f_s}{N_w}$, $\frac{cf_s}{N_w}$, and $\frac{(c+1)f_s}{N_w}$.

Theoretically, not only the bin frequencies but also other frequencies can be used in the DFT, and the second harmonic interferences at different frequencies are not the same. In this way, we can find and use frequencies with the smallest second harmonic interferences in the DFT. In the next subsection, these issues are discussed.

B. Accuracy Analysis and Enhancement of the IpD²FT

Consider that the signal $s(t)$ in (1) is stationary. By applying the DFT to $s(t)$ with a cosine-class window (see Appendix), we can obtain

$$S = \frac{\sqrt{2}}{2} a_1 e^{j\varphi_1} \cdot D(f_b - f) \cdot R(f_b - f) \quad (9)$$

$$+ \frac{\sqrt{2}}{2} a_1 e^{-j\varphi_1} \cdot D(f_b + f) \cdot R(f_b + f)$$

$$+ \frac{\sqrt{2}}{2} a_2 e^{j\varphi_2} \cdot D(f_b - 2f) \cdot R(f_b - 2f)$$

$$+ \frac{\sqrt{2}}{2} a_2 e^{-j\varphi_2} \cdot D(f_b + 2f) \cdot R(f_b + 2f)$$

where

$$D(f) = \frac{\sin \frac{\pi N_w f}{f_s}}{N_w \sin \frac{\pi f}{f_s}} \quad (10)$$

is the Dirichlet kernel; and

$$R(f) = \sum_{m=0}^{M-1} \frac{x_m(-1)^m \cos \frac{m\pi}{N_w}}{[1 - \sin^2(\frac{m\pi}{N_w})/\sin^2(\frac{\pi f}{f_s})]} \quad (11)$$

is a function corresponding to the window function. According to (9), S can be divided into four components, which are the positive and negative fundamental components, positive and negative second harmonic components, respectively (see Fig. 1). Because the positive and negative fundamental components are considered in the signal model of the IpD²FT, its estimation error is mainly caused by the positive and negative

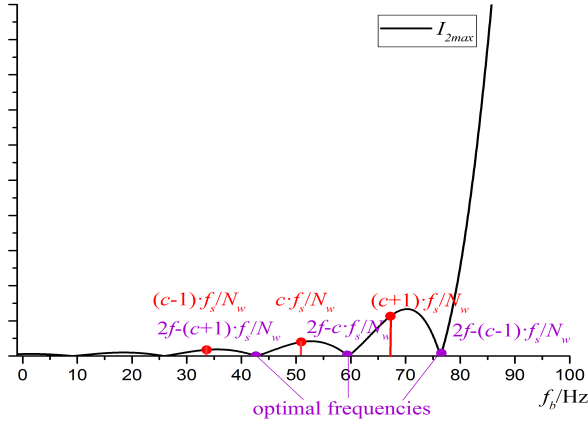


Fig. 2. The maximum interferences caused by the second harmonic component. $\frac{(c-1)f_s}{N_w}$, $\frac{cf_s}{N_w}$, and $\frac{(c+1)f_s}{N_w}$ ($c = 3$) are the three bin frequencies used in the IpD²FT; $2f - \frac{(c+1)f_s}{N_w}$, $2f - \frac{cf_s}{N_w}$, and $2f - \frac{(c-1)f_s}{N_w}$ are the frequencies with the smallest second harmonic interferences. $f_0 = 50$ Hz, $f = 55$ Hz, $N_0 = 40$, and the Hanning window are selected for the illustration.

second harmonic components. Define the second harmonic interference as

$$S_2 = \frac{\sqrt{2}}{2} a_2 e^{j\varphi_2} \cdot D(f_b - 2f) \cdot R(f_b - 2f) + \frac{\sqrt{2}}{2} a_2 e^{-j\varphi_2} \cdot D(f_b + 2f) \cdot R(f_b + 2f) \quad (12)$$

Then, the maximum interference caused by the second harmonic can be given by

$$S_{2max} = \frac{\sqrt{2}}{2} a_2 |D(f_b - 2f)| \cdot |R(f_b - 2f)| + \frac{\sqrt{2}}{2} a_2 |D(f_b + 2f)| \cdot |R(f_b + 2f)| \quad (13)$$

Observe that when $0 < f_b < 100$ Hz, $D(f_b + 2f) \approx 0$. Then (13) can be approximately expressed as

$$S_{2max} \approx \frac{\sqrt{2}}{2} a_2 |D(f_b - 2f)| \cdot |R(f_b - 2f)| \quad (14) \quad 0 < f_b < 100 \text{ Hz}$$

Note that, in general, if

$$f_b = \begin{cases} 2f - \frac{(c-1)f_s}{N_w} \\ 2f - \frac{cf_s}{N_w} \\ 2f - \frac{(c+1)f_s}{N_w} \end{cases} \quad (15)$$

are used in the DFT with a c -cycle M -term cosine-class window ($M \leq 2$), then

$$|D(f_b - 2f)| = 0 \quad (16)$$

$$S_{2max} \approx 0 \quad (17)$$

That is to say, when these frequencies are used in the DFT, the second harmonic interferences are the smallest. However,

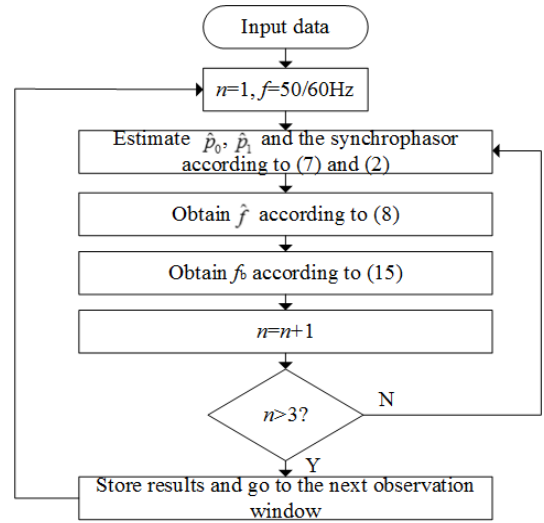


Fig. 3. The implementation steps of the IIPD²FT.

not the frequencies in (15) but the bin frequencies are used in the IpD²FT, which makes it suffer from large second harmonic interferences (see Fig. 2).

Based on this, the IIPD²FT can be proposed by using these three frequencies. It should be noted that, in a practical application, the fundamental frequency f is unknown. Three iterations are also needed to obtain these frequencies. Accordingly, the implementation steps of the IIPD²FT are given in Fig. 3.

III. SIMULATION TESTS

In order to evaluate the performances of the IIPD²FT and IpD²FT, several simulation tests under different test types are taken. The tests are carried out over 50 fundamental cycles with 40 samples per cycle for a 50-Hz system. $T_w = 3/f_0$ are selected in all simulation tests, and the Hanning window is used in both estimators. The total vector error (TVE), frequency error (FE) (an absolute value), and response time defined in the IEEE standard C37.118.1-2011 [15] (called the standard in the following) are the coefficients used to evaluate the performances of both estimators. All the reference values are set according to the M class requirements of the standard and its amendment standard C37.118.1a-2014 [16], with reporting rates $RR \geq 20$ fps.

A. Frequency Deviation Tests

The test signal is shown in (18), f is the fundamental frequency, which is set at 45, 47, 49, 51, 53, and 55 Hz, respectively; and a is the amplitude of the second harmonic component, which is set at 0, 0.05, and 0.1, respectively.

$$s(t) = \cos(2\pi ft) + a \cos(2\pi \cdot 2f \cdot t) \quad (18)$$

The maximum TVEs and |FE|s obtained with the IIPD²FT and the IpD²FT are given in TABLE I. From TABLE I, we can see that the IIPD²FT can sufficiently suppress the second harmonic interferences, even under large frequency deviation

TABLE I
 MAXIMUM TVEs AND |FE|S OBTAINED WITH THE IIPD²FT AND IPD²FT. THE
 REFERENCE VALUE OF THE MAXIMUM TVE AND |FE| IN THE STANDARD ARE 1% AND 25 mHz, RESPECTIVELY. THE GRAY CELLS REPRESENT THE
 RESULTS OUT OF THE RANGE OF THE REQUIREMENTS OF THE STANDARD.

Test type	TVE (%)						FE (mHz)					
	IIPD ² FT			IPD ² FT			IIPD ² FT			IPD ² FT		
	$a = 0$	$a = 0.05$	$a = 0.1$	$a = 0$	$a = 0.05$	$a = 0.1$	$a = 0$	$a = 0.05$	$a = 0.1$	$a = 0$	$a = 0.05$	$a = 0.1$
$f = 45\text{Hz}$	0.00	0.02	0.04	0.00	1.20	2.41	0.00	0.97	4.99	0.00	52.79	108.59
$f = 47\text{Hz}$	0.00	0.02	0.04	0.00	0.54	1.08	0.00	1.93	3.65	0.00	38.01	76.70
$f = 49\text{Hz}$	0.00	0.02	0.03	0.00	0.15	0.30	0.00	1.67	3.19	0.00	14.22	28.50
$f = 51\text{Hz}$	0.00	0.02	0.03	0.00	0.06	0.12	0.00	0.90	1.95	0.00	6.29	12.58
$f = 53\text{Hz}$	0.00	0.02	0.03	0.00	0.13	0.26	0.00	0.77	1.29	0.00	16.97	34.00
$f = 55\text{Hz}$	0.00	0.02	0.03	0.00	0.11	0.23	0.00	0.80	0.59	0.00	16.66	33.37

conditions. As a result, even under these large disturbances, the IIPD²FT can still fully meet the M class requirements of the standard. However, when the signal has significant second harmonic interferences, the maximum TVEs of the IPD²FT are very large, and are out of the range of the requirements of the standard under some conditions. For example, if $f=45$ Hz and $a=0.1$, the maximum TVE reaches 2.41%, which is much larger than the requirements of the standard (1%). Similar conclusions can be drawn in frequency estimation (see TABLE I). The IIPD²FT can fully meet the requirements of the standard, and it is much more accurate than the IPD²FT.

B. Power Oscillation Tests

The estimators' performances under power oscillations, frequency deviations, and second harmonic interferences are tested. The test signal is shown in (19), where $f = 55$ Hz is the fundamental frequency; $a = 0.1$ is the amplitude of the second harmonic component; $k_x = 0.1$ and $k_a = 0.1$ are the amplitude and phase modulation factors respectively; and f_m is the modulation frequency, which is set at 1, 2, ..., 5, Hz respectively.

$$s(t) = (1 + k_x \cos(2\pi f_m t)) \cos(2\pi f t + k_a \cos(2\pi f_m t)) + a \cos(2\pi \cdot 2f \cdot t) \quad (19)$$

The results are shown in Fig. 4, Fig. 5, and TABLE II. From Figs. 4 and 5, we can see that the estimated amplitudes and frequencies obtained with the IIPD²FT are close to the theoretical value. However, the estimated values obtained with the IPD²FT have some fluctuations around the theoretical value. From TABLE II, we can conclude that, even under power oscillations, large second harmonic interferences and frequency deviations, the IIPD²FT can still meet the requirements, and it is much more accurate than the IPD²FT.

C. Other Performance Tests

Other test types in the standard, such as step change tests and frequency ramping tests, are also tested. The results are shown in TABLE III. Note that the performances of the IIPD²FT and IPD²FT are almost the same. In the frequency ramping test, the maximum TVE (%) and |FE| (mHz) of the

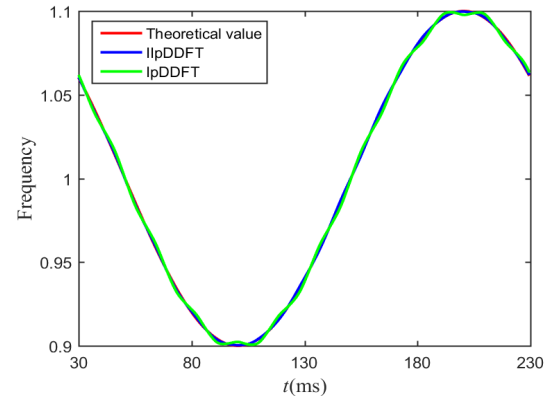


Fig. 4. The theoretical and estimated fundamental amplitudes obtained with IIPD²FT and IPD²FT.

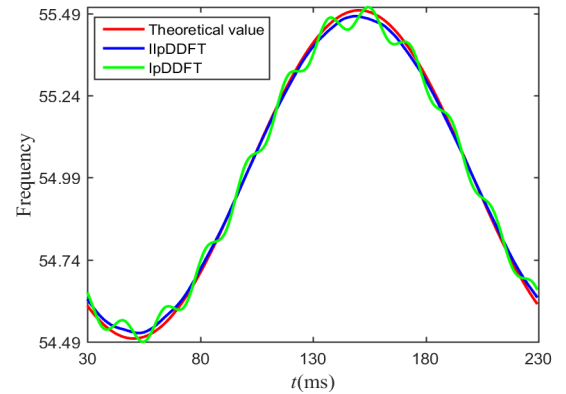


Fig. 5. The theoretical and estimated fundamental frequencies obtained with IIPD²FT and IPD²FT.

IIPD²FT are much smaller than the reference values. Additionally, the same conclusions can be drawn in the amplitude and phase step change tests. From this evidence, we can conclude that, even concerning the performance under step change and frequency ramping conditions, the IIPD²FT can also meet the M class requirements of the standard.

TABLE II
MAXIMUM TVEs AND |FE|S OBTAINED WITH THE IIPD²FT AND IPD²FT. THE REFERENCE VALUES OF THE MAXIMUM TVEs (%) AND |FE|S IN THE STANDARD ARE 3% AND 300 mHz, RESPECTIVELY.

f_m (Hz)	TVE (%)		FE (mHz)	
	IIPD ² FT	IPD ² FT	IIPD ² FT	IPD ² FT
1	0.05	0.25	1.39	37.03
2	0.07	0.25	3.12	37.01
3	0.09	0.25	6.75	38.60
4	0.11	0.26	13.16	43.98
5	0.14	0.27	23.15	53.04

TABLE III
PERFORMANCES OF THE IIPD²FT AND IPD²FT UNDER DIFFERENT TEST TYPES. THE RESPONSE TIME IS EXPRESSED IN NOMINAL SIGNAL CYCLES.

Test type	Indices	TVE (%)			FE (mHz)		
		Std.	IIPD ² FT	IPD ² FT	Std.	IIPD ² FT	IPD ² FT
Freq. ramp	Maximum error	1	0.00	0.00	10	0.00	0.00
Phase step	Response time	7	2.03	2.00	14	2.15	2.45
Amp. step	Response time	7	0.80	0.78	14	2.33	2.30

IV. CONCLUSION

This paper proposes an improved dynamic synchrophasor estimator for large second harmonic interference conditions. The estimation errors caused by second harmonic interferences are mainly divided into the positive and negative second harmonic frequency components. The optimal frequencies for interpolation are obtained based on these analysis results. Even under large frequency deviation and power oscillation conditions, the IIPD²FT can also sufficiently suppress second harmonic interferences, and it is much more accurate than the IPD²FT. Moreover, even for step change and frequency ramping test, the IIPD²FT can still meet the M class requirements of the standard.

APPENDIX

After being sampled, a stationary harmonic component can be expressed as

$$s_h(n) = \sqrt{2}a_h \cos(2\pi \cdot hf \cdot n/f_s + \varphi_h) \quad (\text{A1})$$

where h is the harmonic order. Applying the windowed DFT to (A1) at frequency f_b , it follows that

$$S_h = \frac{1}{N_w} \sum_{n=-N}^N s_2(n)w(n)e^{-j2\pi f_b n/f_s} \quad (\text{A2})$$

If a cosine-class window

$$w(n) = \sum_{m=0}^{M-1} x_m \cos\left(\frac{2\pi mn}{N_w}\right) \quad (\text{A3})$$

with M terms is used in (A2) [5], then it can be rearranged as

$$\begin{aligned} S_h &= \frac{\sqrt{2}a_h}{2N_w} e^{j\varphi_h} \times \\ &\sum_{m=0}^{M-1} \sum_{n=-N}^N \frac{e^{-j\frac{2\pi n}{f_s}[(f_b-hf)-m]} + e^{-j\frac{2\pi n}{f_s}[(f_b-hf)+m]}}{2} \\ &+ \frac{\sqrt{2}a_h}{2N_w} e^{-j\varphi_h} \times \\ &\sum_{m=0}^{M-1} \sum_{n=-N}^N \frac{e^{-j\frac{2\pi n}{f_s}[(f_b+hf)-m]} + e^{-j\frac{2\pi n}{f_s}[(f_b+hf)+m]}}{2} \\ &= \frac{\sqrt{2}}{2} a_h e^{j\varphi_h} \cdot D(f_b - hf) \cdot R(f_b - hf) \\ &+ \frac{\sqrt{2}}{2} a_h e^{-j\varphi_h} \cdot D(f_b + hf) \cdot R(f_b + hf) \end{aligned} \quad (\text{A4})$$

where

$$D(f) = \frac{\sin \frac{\pi N_w f}{f_s}}{N_w \sin \frac{\pi f}{f_s}} \quad (\text{A5})$$

is the Dirichlet kernel; and

$$R(f) = \sum_{m=0}^{M-1} \frac{x_m (-1)^m \cos \frac{m\pi}{N_w}}{[1 - \sin^2(\frac{m\pi}{N_w})/\sin^2(\frac{\pi f}{f_s})]} \quad (\text{A6})$$

is a function corresponding to the window function.

REFERENCES

- [1] J. A. D. L. O. Serna, "Dynamic phasor estimates for power system oscillations," *IEEE Transactions on Instrumentation and Measurement*, vol. 56, no. 5, pp. 1648–1657, 2007.
- [2] M. A. Platas-Garza, J. Platas-Garza, and J. A. D. L. O. Serna, "Dynamic phasor and frequency estimates through maximally flat differentiators," *IEEE Transactions on Instrumentation and Measurement*, vol. 59, no. 7, pp. 1803–1811, 2010.
- [3] S. Vejdan, M. Sanaye-Pasand, and O. P. Malik, "Accurate dynamic phasor estimation based on the signal model under off-nominal frequency and oscillations," *IEEE Transactions on Smart Grid*, vol. 8, no. 2, pp. 708–719, 2017.
- [4] M. Pelekis and K. Krishnan, "Enhanced interpolated-DFT for synchrophasor estimation in fpgas: Theory, implementation, and validation of a pmu prototype," *IEEE Transactions on Instrumentation and Measurement*, vol. 63, no. 12, pp. 2824–2836, 2014.
- [5] D. Macii, D. Petri, and A. Zorati, "Accuracy analysis and enhancement of dft-based synchrophasor estimators in off-nominal conditions," *IEEE Transactions on Instrumentation and Measurement*, vol. 61, no. 10, pp. 2653–2664, 2012.
- [6] D. Petri, D. Fontanelli, and D. Macii, "A frequency-domain algorithm for dynamic synchrophasor and frequency estimation," *IEEE Transactions on Instrumentation and Measurement*, vol. 63, no. 10, pp. 2330–2340, 2014.
- [7] D. Belega, D. Fontanelli, and D. Petri, "Dynamic phasor and frequency measurements by an improved taylor weighted least squares algorithm," *IEEE Transactions on Instrumentation and Measurement*, vol. 64, no. 8, pp. 2165–2178, 2015.
- [8] D. Belega and D. Petri, "Accuracy analysis of the multicycle synchrophasor estimator provided by the interpolated DFT algorithm," *IEEE Transactions on Instrumentation and Measurement*, vol. 62, no. 5, pp. 942–953, 2013.
- [9] R. K. Mai, Z. Y. He, L. Fu, B. Kirby, and Z. Q. Bo, "A dynamic synchrophasor estimation algorithm for online application," *IEEE Transactions on Power Delivery*, vol. 25, no. 2, pp. 570–578, 2010.
- [10] T. Bi, H. Liu, Q. Feng, C. Qian, and Y. Liu, "Dynamic phasor model-based synchrophasor estimation algorithm for m-class pmu," *IEEE Transactions on Power Delivery*, vol. 30, no. 3, pp. 1162–1171, 2015.

- [11] L. Zhan, Y. Liu, and Y. Liu, "A clarke transformation-based DFT phasor and frequency algorithm for wide frequency range," *IEEE Transactions on Smart Grid*, vol. PP, no. 99, pp. 1–1, 2016.
- [12] F. Ling, J. Zhang, S. Xiong, Z. He, and R. Mai, "A modified dynamic synchrophasor estimation algorithm considering frequency deviation," *IEEE Transactions on Smart Grid*, vol. PP, no. 99, pp. 1–1, 2017.
- [13] M. A. Platas-Garza and J. A. D. L. O. Serna, "Dynamic harmonic analysis through taylorfourier transform," *IEEE Transactions on Instrumentation and Measurement*, vol. 60, no. 3, pp. 804–813, 2011.
- [14] D. Dotta and J. H. Chow, "Second harmonic filtering in phasor measurement estimation," *IEEE Transactions on Power Delivery*, vol. 28, no. 2, pp. 1240–1241, April 2013.
- [15] "IEEE standard for synchrophasor measurements for power systems," *IEEE Std C37.118.1-2011 (Revision of IEEE Std C37.118-2005)*, pp. 1–61, Dec 2011.
- [16] "IEEE standard for synchrophasor measurements for power systems – amendment 1: Modification of selected performance requirements," *IEEE Std C37.118.1a-2014 (Amendment to IEEE Std C37.118.1-2011)*, pp. 1–25, April 2014.